A major purpose of the Technical Information Center is to provide the broadest dissemination possible of information contained in DOE's Research and Development Reports to business, industry, the academic community, and federal, state and local governments.

Although a small portion of this report is not reproducible, it is being made available to expedite the availability of information on the research discussed herein.

1

LA-UR-84-1293
CONF

NOTICE

PORTIONS OF THIS REPORT ARE ILLEGIBLE. It has been reproduced from the best available copy to permit the broadest possible availability.

Los Alamos National Laboratory is operated by the University of California for the United States Department of Energy under contract W-7405-ENG-36.

CONF-8403112--4

LA-UR--84-1293

DE84 011383

TITLE STUDY OF GIANT RESONANCES WITH PIONS

AUTHOR(S): Helmut W. Baer

SUBMITTED TO. International Symposium on Nuclear Spectroscopy and Nuclear Interactions, Osaka, Japan, March 21-24, 1984.

DISCLAIMER

This report was prepared as an account of work sponsored by an agency of the United States Government. Neither the United States Government nor any agency thereof, nor any of their employees, makes any warranty, express or implied, or assumes any legal liability or responsibility for the accuracy, completeness, or usefulness of any information, apparatus, product, or process disclosed, or represents that its use would not infringe privately owned rights. Reference herein to any specific commercial product, process, or service by trade name, trademark, manufacturer, or otherwise does not necessarily constitute or imply its endorsement, recommendation, or favoring by the United States Government or any agency thereof. The views and opinions of authors expressed herein do not necessarily state or reflect those of the United States Government or any agency thereof.

MASTER

By acceptance of this article, the publisher recognizes that the U S Government retains a nonexclusive, royalty-free license to publish or reproduce the published form of this contribution, or to allow others to do so, for U S Government purposes.

The Los Alamos National Laboratory requests that the publisher identify this article as work performed under the auspices of the U S Department of Energy

Los Alamos National Laboratory
Los Alamos, New Mexico 87545

FORM NO 836 R4
ST NO 2629 5/81

STUDY OF GIANT RESONANCES WITH PIONS

Helmut W. Baer
Medium-Energy Physics Division
Los Alamos National Laboratory, Los Alamos, NM 87545

ABSTRACT

Recent results on giant resonances obtained with pion-inelastic scattering and with single- and double-charge-exchange scattering are reviewed. The states discussed are isobaric analog states, double-isobaric analog states, and isovector L = 0, 1, and 2 collective states.

I. INTRODUCTION

An isobar diagram illustrating the general features of pion scattering on $N > Z + 2$ nuclei is shown in Fig. 1. Pion scattering is unique in three respects: (1) The pion is the only elementary particle used by nuclear physicists that comes in three charge states, π^+, π^0, and π^-. This leads to the study of the double isobaric analog state (DIAS). (2) The pion is a spin-zero boson. Thus one has "true absorption" and "true creation" of pions in pion-scattering phenomena. This leads to the study of nucleon resonances embedded in nuclei. (3) The π-N system has a pronounced, isolated resonance, the Δ_{33},

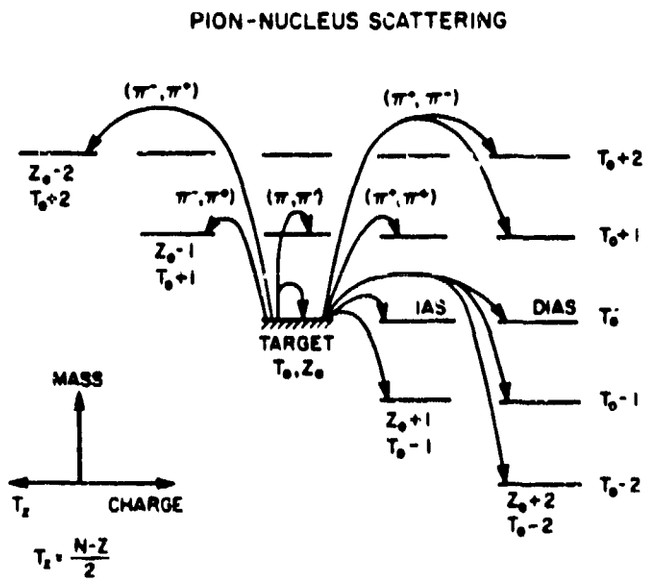

Fig. 1. Isobar diagram illustrating the range of scattering phenomena possible with pions.

which exists in four charge states, Δ^{++}, Δ^{+}, Δ^{o}, and Δ^{-} (T = 3/2), and which causes the scattering of π^{+} and π^{-} on nuclei to be quite different. This leads to pronounced differential sensitivity to neutron and proton transition densities in inelastic pion scattering.

We review here the status of experiments and theory for the giant resonances that are being studied with pions:

TABLE I. GIANT RESONANCES BEING STUDIED WITH π's

Resonance Name	ΔL	Reactions	Transition Density (1st Approx.)	Strong-Absorption $d\sigma/d\Omega$ Shape
IAS	0	(π^{+},π^{0})	ρ_{exc} $(\approx\rho_{\bar{n}}\rho_{p})$	$J_0^2(x)$
DIAS	0	(π^{+},π^{-})	ρ_{exc}^2	$[J_0 - \beta(J_0 - xJ_1)]^2$
IV-GMR	0	$(\pi^{\pm},\pi^{0})$	$3\rho + r\, d\rho/dr$	J_0^2
IV-GDR	1	$(\pi^{\pm},\pi^{0})$	$d\rho/dr$	J_1^2
IV-GQR	2	$(\pi^{\pm},\pi^{0})$	$r\, d\rho/dr$	$1/4\ J_0^2 + 3/4\ J_2^2$
IS-GQR	2	(π,π')	$r\, d\rho/dr$	$1/4\ J_0^2 + 3/4\ J_2^2$
π^{+} ELASTIC	0	π^{+}	$\sim(\rho_n + 3\rho_p)$	$J_1(x)/x$
π^{-} ELASTIC	0	π^{-}	$\sim(3\rho_n + \rho_p)$	$J_1(x)/x$

$x = q\bar{R} \approx (2k \sin\frac{\theta}{2})\bar{R}$; $\bar{R} \approx 1.35\ A^{1/3}$ fm (effective impact parameter).

Included in this list are the isobaric analog state (IAS) and the DIAS. In heavier nuclei where the neutron excess is large, these are truly collective states in that the transition amplitudes involved are coherent sums over the many orbitals of the excess neutrons. Also given in Table I are the collective-model transition densities and analytical formulas for the angular-distribution shapes. Since a dominant feature of pion-nucleus scattering at beam energies between 100 and 300 MeV is strong absorption of pions, an eikonal approximation to the scattering amplitudes can be made.[1] This leads to analytical formulas[1,2] for the differential cross sections involving Bessel functions. These formulas give a good first approximation to the measured angular-distribution shapes at forward-scattering angles.

II. IAS AND DIAS RESULTS

A. Isobaric Analog States (IAS)

A good example of a giant resonance is shown in Fig. 2. The IAS is the most prominent feature of the spectrum[3] of the reaction $^{90}Zr(\pi^+,\pi^0)^{90}Nb$ at forward angles. To appreciate the selectivity of the (π^+, π^0) reaction to the IAS one should note that if the π^0 spectrum for this reaction had been measured with a resolution of 100 keV, a typical number for charged particle detectors, the IAS peak would be approximately 4 m high sitting on a background of 4 cm. To the best of our knowledge no other discrete states would contribute substantially to the 0° spectrum. Thus the (π^+,π^0) reaction at $q = 0$ is a good physical realization of the isospin ladder operator, $T_- = \frac{1}{\sqrt{2j+1}} \sum_{jm} a^+_{jm}(p)\, a_{jm}(n)$.

Experiments in Los Alamos performed in the past few years have measured the general systematics of 0° IAS cross sections[3-5] for a series of nuclei ranging from ^7Li to ^{208}Pb and angular distributions[6,7] for ^{13}C and ^{15}N. The 0° cross sections for 165 MeV are shown in Fig. 3. Similar results are available[5] at 100, 230, and 295 MeV. The 0° differential cross sections are described quite well by the function $g(E)(N - Z)A^{-\alpha(E)}$. The value of α expected at 165 MeV from a strong-absorption model (discussed below) is 4/3. A fit to 165-MeV data yields[5] $\alpha = 1.35 \pm 0.04$. This function shown in Fig. 3 is seen to reproduce the trend of the data quite well. The available data show α to

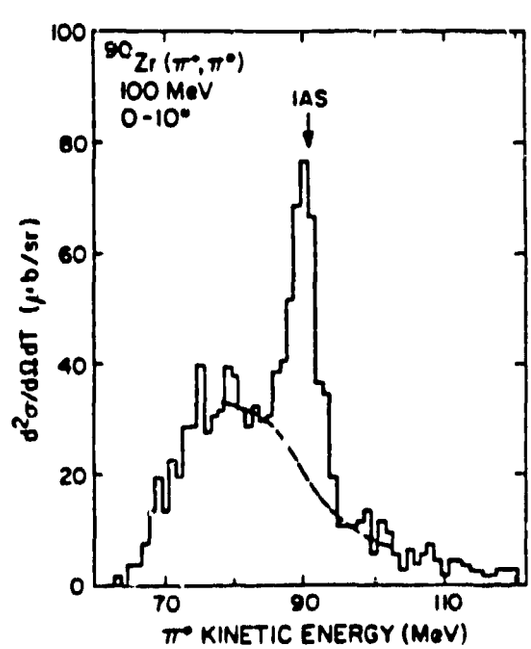

Fig. 2. Neutral-pion spectrum measured with the LAMPF π^0 spectrometer. The isobaric analog state (IAS) is a prominent feature of all (π^+,π^0) spectra on $N > Z$ nuclei at incident energies 100 to 300 MeV.

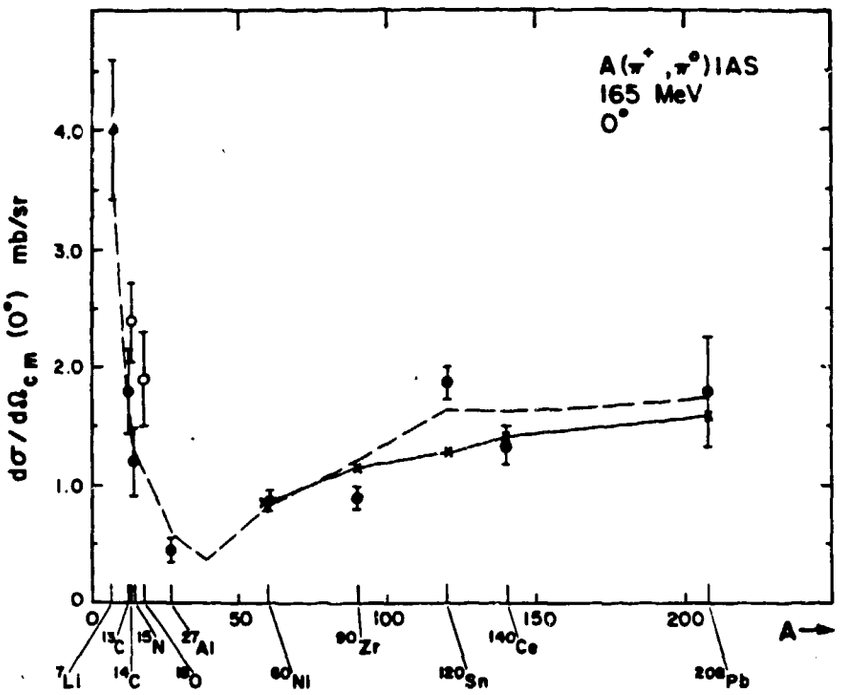

Fig. 3. The A dependence of 0° differential cross sections for the IAS state. The dashed line represents the function $49(N - Z)A^{-4/3}$ mb/sr. The solid line represents recent calculations[8,9] performed with second-order optical potentials and Hartree-Fock density distributions.

be a decreasing function of energy. At 295 MeV the value is $\alpha = 1.10 \pm 0.03$. This reflects the increased volume scattering at higher energies. The energy dependence of g(E) follows quite closely the energy dependence of the 0° free-nucleon charge-exchange cross section.

An example of a 0° excitation function[4] is shown in Fig. 4. We note the similarity between the $^{7}Li(\pi^{+},\pi^{0})^{7}Be$ (IAS) reaction to the $\pi^{-}p \rightarrow \pi^{0}n$ reaction over the broad energy interval 30 to 300 MeV. This is strong evidence that the essential character of the charge-exchange interaction is not modified by the nuclear medium. The results of two current theoretical analyses using different scattering theories[9,10] are compared to the data. Neither approach describes well the energy dependence over the full range.

B. Double Isobaric Analog States (DIAS)

The study of DIAS transitions with an elementary particle is a new dimension in nuclear studies made possible by high-intensity pion beams. Survey experiments to determine the energy- and A-dependence of forward-angle DIAS cross sections were performed at EPICS in the past few years. The nuclear-structure simplifications one has in DIAS transitions, namely,

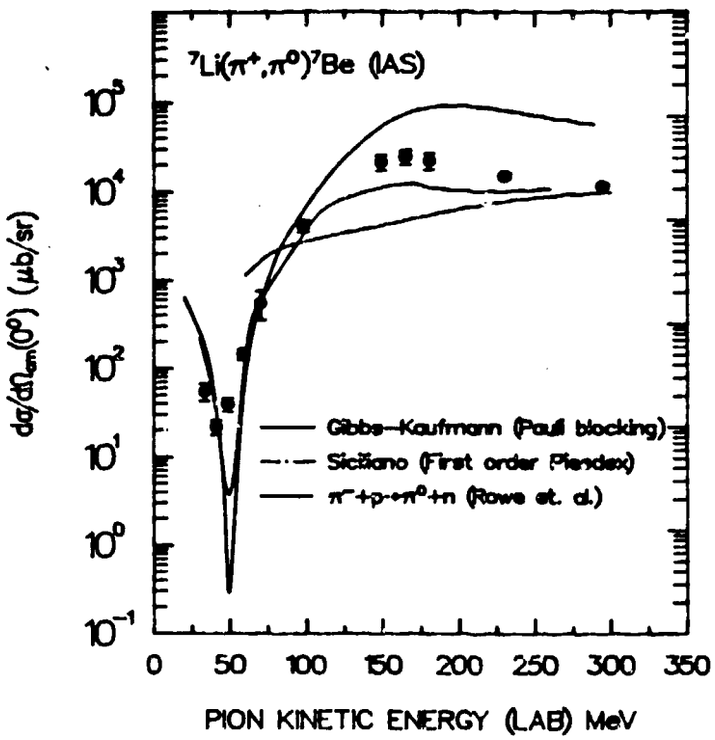

Fig. 4. Energy dependence of the 0° differential cross section for the IAS state. Comparison is made to two theoretical calculations[9,10] based on two different scattering theories, and to the free two-body process. The IAS data[4] are seen to retain the qualitative features of the elementary $\pi^- p \to \pi^0 n$ cross section.

$|DIAS\rangle = [(N - Z)(N - Z - 1)]^{-1}\, T_- T_- |TARGET\rangle$, make these transitions most suitable for initial studies of reaction mechanisms.

The experiments show that the DIAS transition must be studied at the highest possible energies, near 300 MeV for EPICS, if the data are to extend throughout the periodic table. Spectra measured[11,12] for ^{14}C, ^{56}Fe, and ^{209}Bi are shown in Fig. 5(a-c). In ^{14}C as well as other light $N = Z + 2$ nuclei, the DIAS is the strongest transition at forward angles for beam energies between 160 and 295 MeV. For medium-mass nuclei such as ^{56}Fe, non-DIAS transitions are stronger at the lower energies. The DIAS cannot be clearly seen at 140 MeV on ^{56}Fe [Fig. 5(b)]. At higher energies (295 MeV) the DIAS again dominates the spectrum of ^{56}Fe and also that of ^{88}Sr (Ref. 13). For ^{209}Bi it becomes difficult to observe the DIAS, even at 295 MeV [Fig. 5(c)]. Thus the DIAS transitions, if they are to be studied in heavy nuclei, must be measured at $T_\pi \gtrsim 300$ MeV.

The excitation energy of the DIAS in ^{209}At is 31 MeV and it appears to be a narrow state ($\Gamma < 1$ MeV). The signal/background for the measurement is approximately 1 to 1 and the differential cross section is $\sigma_{DIAS}(5^o) =$

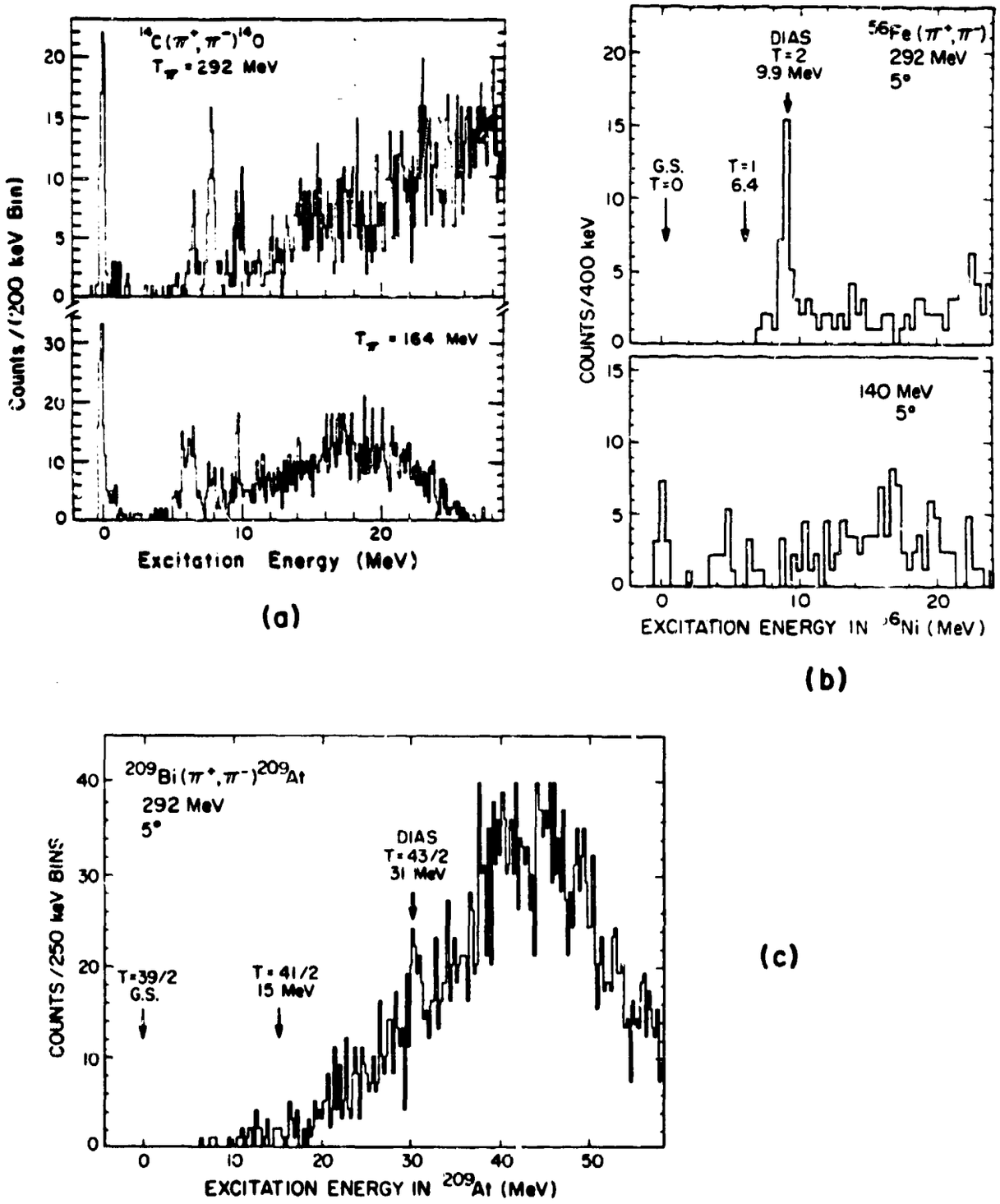

Fig. 5. (a) Measured $^{14}C(\pi^+,\pi^-)$ spectra[11] at 165 and 292 MeV. They are summed spectra for measurements between 0 and 50°. The double isobaric analog state (DIAS) is seen to be the strongest state at both energies. (b) Measured $^{56}Fe(\pi^+,\pi^-)$ spectra at 5° for incident energies of 140 and 292 MeV. The DIAS state has a small cross section at 140 MeV relative to other states. At 292 MeV it has a large cross section compared to other states. (c) Measured $^{209}Bi(\pi^+,\pi^-)$ spectrum. The spectrum near the ground state (g.s.) was off the focal plane for this measurement.

0.46 ± 0.15 μb/sr. The increasing excitation energy for the DIAS state as a function of A can be seen directly in the (π^+,π^-) spectra of Fig. 5. For ^{14}C, ^{56}Fe, ^{88}Sr, and ^{209}Bi, these are, respectively 0.0, 9.9, 17.4, and 31 MeV and the isospin values are 0, 2, 6, and 43/2, respectively.

The excitation functions for the (π^+,π^-) reactions[11] in the interval 100 to 300 MeV show $\sigma_{DIAS}(5^o)$ to increase with increasing energy. Other $\Delta L = 0$ transitions have decreasing cross sections. Data for $\sigma_{DIAS}(5^o)$ for ^{14}C, ^{18}O, and ^{56}Fe are shown in Fig. 6. We note here a peculiarity found for DIAS transitions, namely, the resonance-like structure in $\sigma_{DIAS}(5^o)$ vs T_π that exists in some cases (^{18}O, Ref. 14) but not in others. The increase in $\sigma_{DIAS}(5^o)$ at the higher energies is what might reasonably be expected, taking into account the increase in the elementary cross sections $\pi^+n \rightarrow \pi^0p$ and $\pi^0n \rightarrow \pi^-p$ and the observed increase in $\sigma_{IAS}(0^o)$ with energy (Fig. 4). Early theoretical calculations anticipated[15] this trend for both $\sigma_{IAS}(0^o)$ and $\sigma_{DIAS}(0^o)$. The resonance-like behavior at lower energies was not expected, and its origin is not fully understood at present.

Several aspects of the data indicate that the reaction mechanism for DIAS transitions simplifies somewhat at the higher energies. The A dependence of the reduced cross sections $\sigma_{DIAS}(5^o)/(N - Z)(N - Z - 1)$ is shown for 164 and

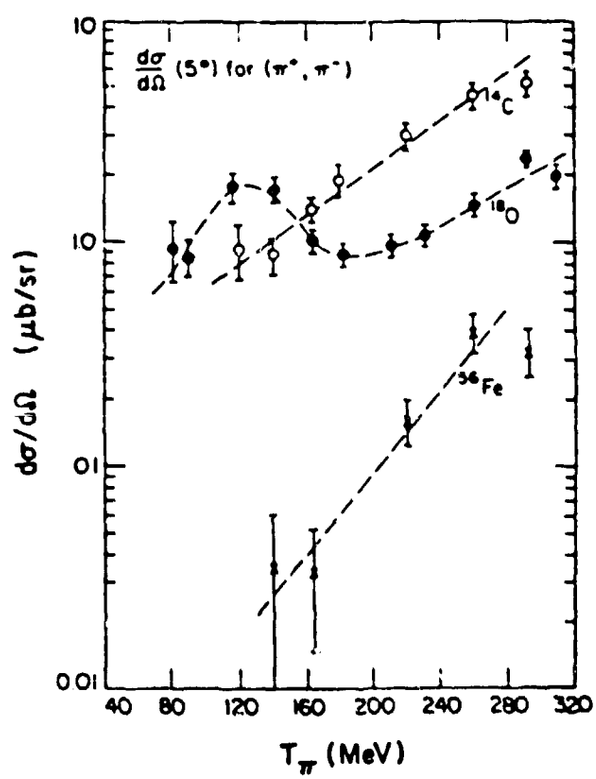

Fig. 6. Excitation functions at 5° for the DIAS state.[11] The functional form at the lower energies is quite different for ^{14}C and ^{18}O.

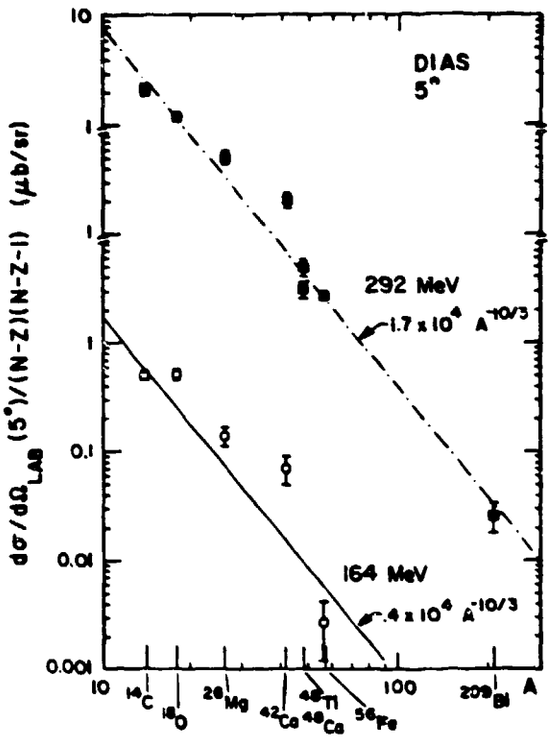

Fig. 7. The A dependence of (π^+,π^-) DIAS differential cross sections at 5°. The straight lines are fits to the data assuming an A dependence of $A^{-10/3}$ as expected for the strong-absorption model.

295 MeV in Fig. 7. At 295 MeV all the data points[11,12,14,16] except ^{42}Ca fall closely to the line given by

$$\frac{d\sigma}{d\Omega}(5^\circ)_{DIAS} = 17\ (N - Z)(N - Z - 1)\ A^{-10/3}\ \text{mb/sr} \quad . \tag{1}$$

This function follows from the strong-absorption model discussed below. A second feature of the 295-MeV data is that the angular-distribution shapes[11] measured for ^{14}C, ^{18}O, ^{26}Mg, and ^{56}Fe have shapes consistent with a diffraction picture for the reaction. The DIAS data at 164 MeV is irregular with respect to A dependence (Fig. 7), angular-distribution shapes, and 5° excitation functions between 100 and 200 MeV (Fig. 6).

The major empirical result to date on DIAS transitions is the measurement of $\sigma_{DIAS}(5^\circ)$ at 295 MeV through the periodic table and the existence of regular patterns in A dependence and angular-distribution shapes in these data. This gives some hope that a simple picture of the reaction picture may be formulated and that comparisons between IAS and DIAS transitions may be

exploited to study the two-nucleon correlations and perhaps even subnucleonic degrees of freedom.

C. Strong-Absorption Model for IAS and DIAS Transitions

Strong-absorption models for pion scattering were developed by Johnson and Bethe[1] and applied to IAS and DIAS transitions by Johnson[2] and Gal.[18] The strong absorption of pions in the energy range 100 to 300 MeV is most directly evident from the sharply oscillating angular-distribution patterns measured for π^+ and π^- elastic scattering. The elastic-scattering amplitude at forward angles is reasonably well approximated by the black disk scattering amplitude $J_1(x)/x$, where $x = q\bar{R} = (2k \sin \theta/2)\bar{R}$ where $\bar{R}$ is disk radius (effective impact parameter). Thus we may use

$$\frac{d\sigma}{d\Omega_{EL}} = N \left(\frac{J_1(x)}{x}\right)^2 , \tag{2}$$

to extract $\bar{R}$ from the position of the measured first minimum. The first zero of this function occurs at $x = 3.83$. The minima are found to occur at $\bar{R} \approx 1.35\ A^{1/3}$ for pion energies near 165 MeV. At this value of $\bar{R}$ the nuclear-density distribution $\rho = \rho_n + \rho_p$ has dropped to 10-20% of its central value. Clearly, elastic scattering and charge-exchange scattering take place at the outer surface of the nucleus.

For IAS transitions the strong-absorption model leads to the expression[2]

$$\frac{d\sigma}{d\Omega_{IAS}} \sim \sigma_{TOT} \left(\frac{1}{\sqrt{2T_0}}\right)^2 \left(\frac{\Delta\rho}{\rho}\right)^2 J_0^2(x) , \tag{3}$$

where $\Delta\rho$ is the excess neutron density ($\approx \rho_n - \rho_p$). The factor $(2T_0)^{-1/2}$ comes from normalization of the IAS wave function $|IAS\rangle = (2T_0)^{-1/2}\ T_-|TARGET\rangle$ when related to the ground state of the target nucleus by the isospin ladder operator. If one further assumes that $\rho_n = (N/Z)\rho_p$ and that $\sigma_{TOT} \sim A^{2/3}$ (disk area), Eq. (3) reduces to

$$\frac{d\sigma}{d\Omega_{IAS}} = g\ \frac{N - Z}{A^{4/3}}\ J_0^2 . \tag{4}$$

A further simplification is possible if one notes[19] that for stable nuclides (bottom of mass parabola),

$$(N - Z) \sim A^{5/3} \quad , \quad A \gtrsim 60 \quad . \tag{5}$$

Thus we expect $\sigma_{IAS}(0^\circ) \sim A^{1/3}$ for heavy nuclei. The data between 100 and 300 MeV are in agreement with these general trends.

For DIAS transitions the strong-absorption model leads to[2]

$$\frac{d\sigma}{d\sigma\Omega}_{DIAS} \sim \sigma_{TOT} \left(\frac{1}{\sqrt{2T_0}} \cdot \frac{1}{\sqrt{2(T_0 - 1)}}\right)^2 \left(\frac{\Delta\rho}{\rho}\right)^4 [J_0 - \beta(J_0 - xJ_1)]^2 \quad . \tag{6}$$

The angular-distribution shape is due to an interference of J_0 or J_1 terms. This can produce a first minimum at a smaller angle than the first minimum of either J_0 or J_1. The value of β is not well determined in the simplest models. The data show that the first minima of DIAS angular distributions are at more forward angles than expected from $J_0(q\bar{R})$ alone, indicating a large value of β. Recent theoretical studies[8,9] show that large values of β arise from the combined effect of second-order terms in the isovector (U_1) and isotensor (U_2) terms of the pion-nucleus optical potential.[8] The positions of the minima are seen as signatures to the role of the isotensor term.

The (N - Z) and A dependence of 0° DIAS cross sections given by this model are

$$\frac{d\sigma}{d\Omega}(0^\circ)_{DIAS} = G \frac{(N - Z)(N - Z - 1)}{A^{10/3}} \quad , \tag{7}$$

where we have assumed $\rho_n = N/Z\ \rho_p$ and $\sigma_{TOT} \sim A^{2/3}$. A fit[17] to the 5° cross sections at 295 MeV gives G = 17 mb. Noting that $(N - Z) \sim A^{5/3}$ for $A \gtrsim 60$, we expect $\sigma_{DIAS}(0^\circ)$ to be constant for heavy nuclei, with a value ≈ 0.5 μb/sr (^{209}Bi). The 295-MeV data follow these strong-absorption signatures most closely (Fig. 7).

III. INELASTIC SINGLE-CHARGE-EXCHANGE SCATTERING

A. Motivations and Early Results

Pion single-charge-exchange scattering (SCX) has significant advantages for study of isovector monopole, dipole, and quadrupole resonances. (1) The use of both (π^+,π^0) and (π^-,π^0) reactions in the same experimental setup allows one to observe directly the isospin splitting of the resonances and the role of the Pauli exclusion principle in the ratios $\sigma(\pi^-,\pi^0)/\sigma(\pi^+,\pi^0)$. Also, having data for both reactions helps in understanding the continuum. (2) The spin-zero of pions suppresses largely the spin-flip ($\Delta S = 1$) transitions at forward angles. Thus $(\pi^\pm,\pi^0)$ studies complement the (p,n) studies, where $\Delta S = 1$ transitions dominate the low-q spectra. (3) The strong absorption of pions leads to sharply oscillating angular-distribution patterns characterized by the angular-momentum transfer (ΔL) and the interaction radius ($\overline{R}$).

In 1982 we began in Los Alamos a series of measurements designed to study the L = 0, 1, and 2 isovector resonances.[20-25] We used the LAMPF π^0 spectrometer mounted in the low-energy pion (LEP) channel. Two examples of our published results are shown in Figs. 8 and 9.

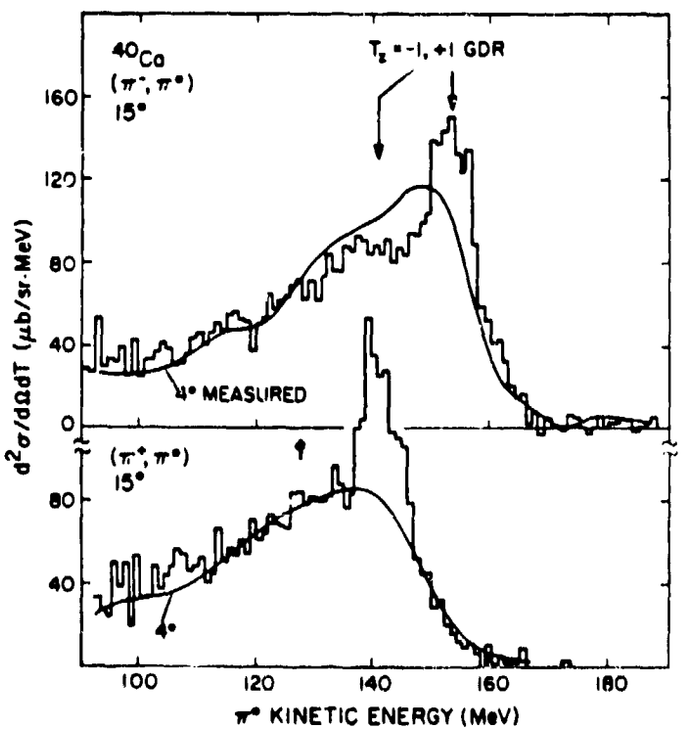

Fig. 8. Comparison of the (π^-,π^0) and (π^+,π^0) spectra for ^{40}Ca. The shift of 12 MeV in the peak of the dipole signal (GDR) is the expected Coulomb displacement energy. The measured (and smoothed) 4° spectra are shown for comparison (solid line). The shape of the (π^-,π^0) spectrum to the left of the GDR (130-150 MeV) is less isotropic than the (π^+,π^0) spectra to the left of the GDR (120-140 MeV).

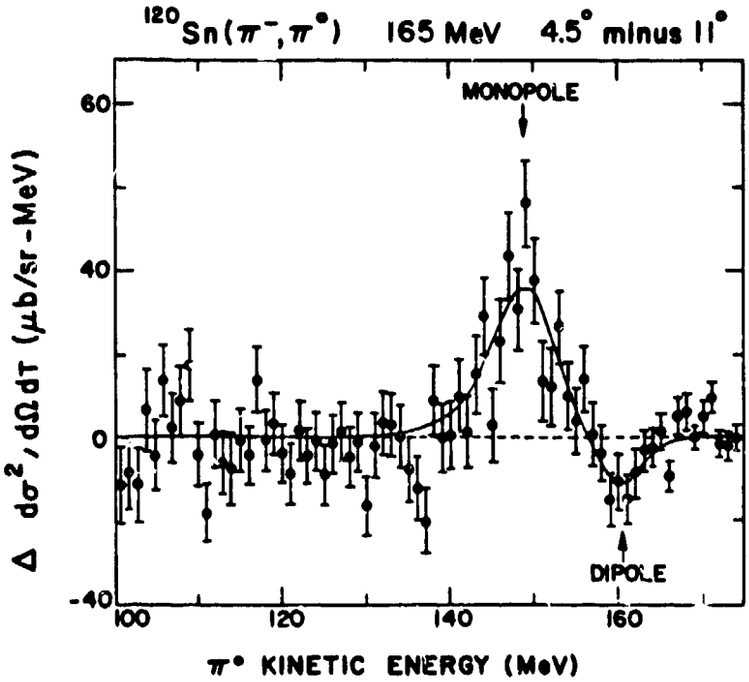

Fig. 9. The monopole and dipole signals as reported in Ref. 21.

The charge-exchange mode of the isovector giant dipole resonance (GDR) is observed as a strong signal in the $^{40}Ca(\pi^{\pm},\pi^0)$ reactions[20] at 165 MeV (Fig. 8). There is a shift of 12 MeV in the π^0 kinetic energy for the GDR peak between the (π^-,π^0) and the (π^+,π^0) reaction. This is exactly the expected shift in the mass of the GDR due to the difference in the electrostatic Coulomb energy between the $M_T = -1$ and $+1$ substates. The expected sharp angular variation of the GDR cross section was also observed. The measured 4° and 30° spectra (Fig. 8) show very little GDR excitation. The $M_T = \pm 1$ GDR states seen in the $(\pi^{\pm},\pi^0)$ spectra are the analogs of the E1 photoabsorption resonance observed at 20 MeV in ^{40}Ca. Unlike the case of the (p,n) reaction where one produces predominantly $\Delta L = 1$, $\Delta S = 1$ transitions and therefore observes largely 2^- states, for the pion charge exchange the $\Delta S = 1$ transitions are small.

We reported[21] the observation of the isovector monopole resonance in the $^{120}Sn(\pi^-,\pi^0)$ and $^{90}Zr(\pi^-,\pi^0)$ reactions. This was based on seeing a forward-peaked feature in the π^0 spectra, as shown for ^{120}Sn in Fig. 9. The measured excitation energy for this peak was 13.8 ± 0.5 MeV in ^{120}Sb, which projects to 31.7 MeV in ^{120}Sn. This is the $T_0 + 1$ component of the monopole state. The width reported was 7 ± 2 MeV and the 0° cross section was 0.58 ± 0.05 mb/sr. A dipole peak was also observed (Fig. 9), corresponding to an excitation energy of 3.3 ± 0.9 MeV in ^{120}Sb.

The data from our first run were analyzed assuming the background under the monopole was isotropic over the angular range 0 to 22°. We have much more extensive data now with more nuclei, larger angular coverage, and detailed spectrometer acceptance measurements. These data show that the background in this angular interval is not strictly isotropic. Thus further study of the background is required to reliably extract giant-resonance parameters.

B. Continuum in SCX

1. General Features of $d^2\sigma/d\Omega dT$ vs θ. The measured π^0 spectra for $^{208}Pb(\pi^{\pm},\pi^0)$ shown in Fig. 10 illustrate some of the general features. At backward-scattering angles (for example, 108°, Ref. 26), there is a broad peak that has been identified with quasi-free (qf) scattering. The center of this peak at 108° is at 65 MeV, which is 30 MeV below the energy for free $\pi^- p \rightarrow \pi^0 n$ scattering. At forward angles the peak of the π^0 spectrum moves to higher energies; at 4° it is approximately 25 MeV below the kinematic limit of ≈165 MeV. This behavior is similar to that observed in inelastic scattering.[27] We note that in the 4° spectra one sees the IAS in (π^+,π^0) but not in (π^-,π^0) scattering. Both the (π^+,π^0) and (π^-,π^0) spectra at forward angles show a long low-energy tail, which extends below 90 MeV.[26] This feature is also present in inelastic scattering, where it was identified[27] with multiply scattered events. We have no calculations for such processes in SCX. It

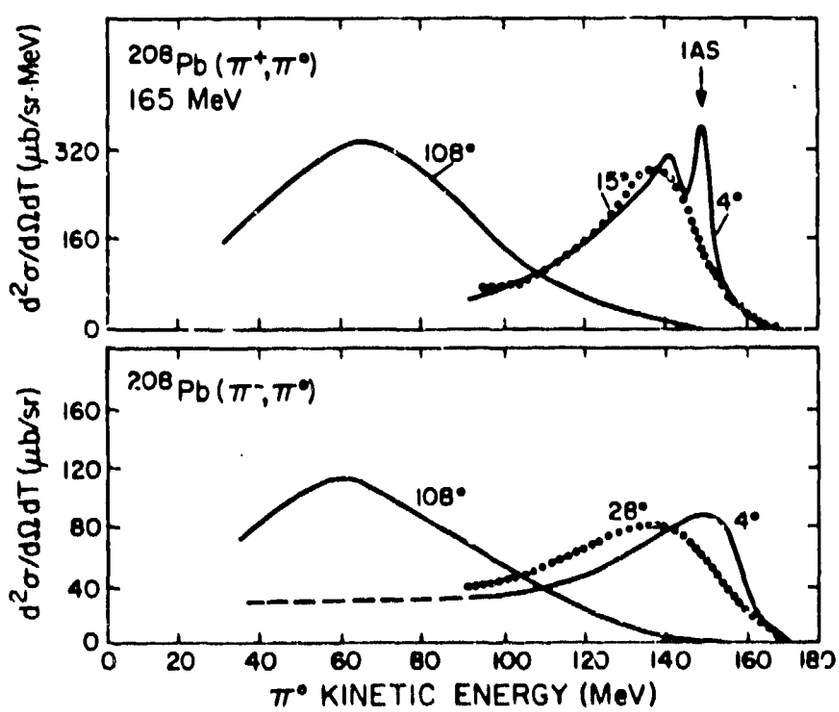

Fig. 10. Measured $^{208}Pb(\pi^{\pm},\pi^0)$ spectra, shown as line traces of the data. The 108° spectra are taken from Ref. 25, the 4° and 15° spectra are from Ref. 22.

seems plausible that the tails in SCX and inelastic scattering are of similar origin.

Both the (π^+,π^-) and (π^-,π^0) inclusive cross sections are largely suppressed[26] at small scattering angles (low q) in comparison to the behavior of the free $\pi^-p \to \pi^0n$ angular-distribution shape. If the shape of $d\sigma/d\Omega$ $(\pi^-p \to \pi^0n)$ is normalized to the backward-angle data[26] on ^{208}Pb, one can obtain a 4° suppression factor, defined as the ratio of the measured 4° energy-integrated cross section to the value at 4° of the normalized $d\sigma/d\Omega(\pi^-p \to \pi^0n)$ curve. For ^{208}Pb this gives for (π^+,π^0) a suppression factor ≈ 0.25 and for (π^-,π^0) the value ≈ 0.15. The suppression is seen to be larger for (π^-,π^0) than for (π^+,π^0). Comparison of the 4° spectra (Fig. 10) shows that the (π^+,π^0) spectrum has a much more pronounced continuum peak than does the (π^-,π^0) spectrum. This may be approximately characterized by the ratio $P \equiv \sigma_{pk}(\sim 142\ \text{MeV};\ 4^\circ)/\sigma(90\ \text{MeV};\ 4^\circ)$. For ^{208}Pb the values are $P(\pi^+) = 5$ for (π^+,π^0) and $P(\pi^-) = 2.5$ for (π^-,π^0).

2. (π^+,π^0) vs (π^-,π^0).

A-dependence of 4° spectra. In Fig. 11 the measured 4° spectra[22] for the $(\pi^\pm,\pi^0)$ reactions on ^{40}Ca and ^{208}Pb are compared. One sees that the two reactions are quite different. The energy-integrated 4° cross sections σ(90 to 165 MeV, 4°) for ^{40}Ca and ^{208}Pb are nearly the same for (π^-,π^0). Also, the $^{208}Pb(\pi^-,\pi^0)$ spectrum shape is flatter than the $^{40}Ca(\pi^-,\pi^0)$ spectrum. For (π^+,π^0) the integrated cross section increases by a factor ~3.5 from ^{40}Ca to ^{208}Pb and the spectrum is more peaked for ^{208}Pb. The A dependence of these properties of the 4° data are given in Table II.

We note the following trends. For the (π^-,π^0) reaction, which converts protons to neutrons, $\sigma(\pi^-)$ vs Z is nearly independent of Z for Z = 20 to 82. Furthermore, the (π^-,π^0) spectra become flatter with increasing A; that is, $P(\pi^-)$ is maximum for ^{40}Ca and minimum for ^{208}Pb. For the (π^+,π^0) reaction, which converts neutrons to protons, $\sigma(\pi^-)$ vs N increases with N. Also, the spectra become more peaked with increasing A, going from $P(\pi^+) = 3.0$ for ^{40}Ca to $P(\pi^+) = 5.0$ for ^{208}Pb.

A similar trend exists[26] for the angle- and energy-integrated inclusive SCX cross sections σ_{SCX}. For ^{16}O, $\sigma_{SCX} = 80 \pm 12$ mb for both (π^+,π^0) and (π^-,π^0); for ^{208}Pb, $\sigma_{SCX} = 252 \pm 30$ mb for (π^+,π^0) and 113 ± 16 mb for (π^-,π^0). Thus σ_{SCX} (π^-,π^0) is nearly constant for ^{16}O to ^{208}Pb, whereas σ_{SCX} (π^+,π^0) increases by a factor of 3 for these nuclei. This near constancy of σ_{SCX} (π^-,π^0) with increasing Z was attributed[26] to screening of the protons by

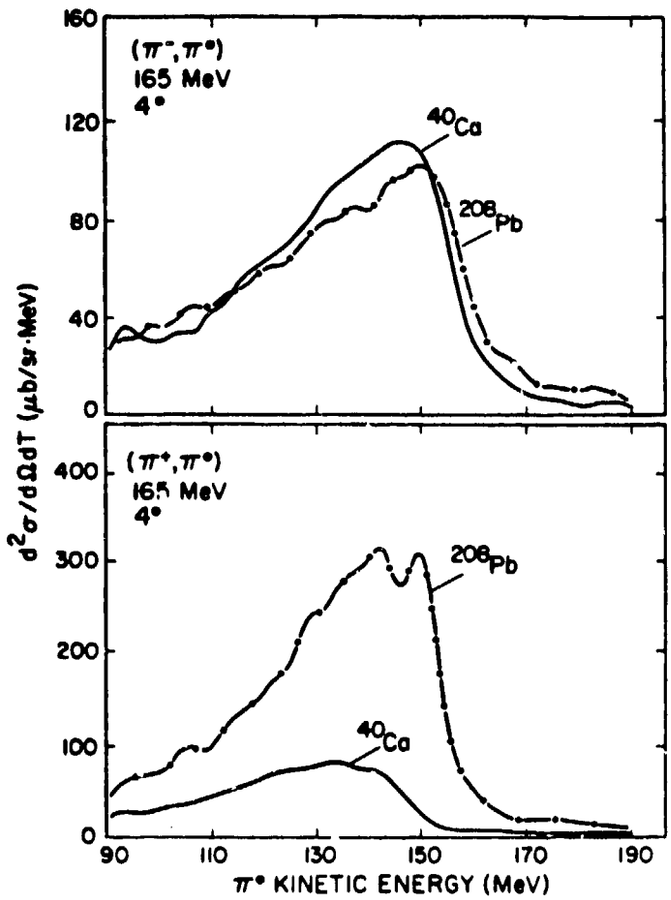

Fig. 11. The A dependence of the measured 4° $(\pi^{\pm},\pi^{0})$ spectra.[22] The (π^{-},π^{0}) spectra for nuclei from ^{40}Ca to ^{208}Pb remain nearly constant, whereas as the (π^{+},π^{0}) spectra show increasing cross sections for the same nuclei.

TABLE II. PROPERTIES OF THE $(\pi^{\pm},\pi^{0})$ SPECTRA AT 4°

A	Z	N − Z	$\sigma(\pi^{-})$ (mb/sr)	$P(\pi^{-})$	$\sigma(\pi^{+})$ (mb/sr)	$P(\pi^{+})$
^{208}Pb	82	44	4.1	2.6	10.9	5.0
^{140}Ce	58	26	4.0	2.7	9.0	3.7
^{120}Sn	50	20	4.0	2.9	9.5	3.7
^{90}Zr	40	10	4.2	3.0	7.8	4.5
^{60}Ni	28	4	5.1	3.3	6.6	3.7
^{40}Ca	20	0	4.4	4.4	3.3	3.0

Estimated errors are approximately 10% for $\sigma(\pi^{\pm})$ and 15% for $Pk(\pi^{\pm})$.

$\sigma(\pi^{\pm})$ = energy-integrated (90 to 165 MeV) spectrum at 4°.

$P(\pi^{\pm})$ = peak value of $d^{2}\sigma/d\Omega dT$ spectrum (near 142 MeV) divided by the 90-MeV value.

the excess neutrons. This screening removes π^- flux through Δ^- formation with subsequent decays out of the π^0 exit channel.

Role of Pauli principle. In the 4° spectra the Pauli principle must play an important role in producing the differences in the (π^-,π^0) and (π^+,π^0) reactions. In Fig. 12 we illustrate the situation for a heavy nucleus. Two classes of excitations are possible in (π^+,π^0) but not in (π^-,π^0)--the 0-$\hbar\omega$ excitations that include the IAS and many other positive-parity states and the 1-$\hbar\omega$ excitations that include the GDR and many other negative-parity states. These classes of excitations require the lowest orbital rearrangement and therefore may be expected to have the largest low-q cross sections. They are largely blocked in (π^-,π^0) on heavy nuclei. The (π^-,π^0) reaction on heavy nuclei must proceed through 2-$\hbar\omega$ excitations coupled to isospin $T_0 + 1$.

The greater peaking of the (π^+,π^0) 4° spectra compared to the (π^-,π^0) 4° is most probably due to the large contributions from 0-$\hbar\omega$ and 1-$\hbar\omega$ excitations. This makes more difficult the observation in (π^+,π^0) reactions of 2-$\hbar\omega$ excitations such as giant monopole and quadrupole resonances.

N = Z nuclei. The only such nucleus included in our survey measurements at 165 MeV is ^{40}Ca. We see in the 4° spectra (Fig. 13) surprisingly large deviations from what is expected from charge symmetry, namely, $\sigma(\pi^+,\pi^0) = \sigma(\pi^-,\pi^0)$. We find $\sigma(\pi^-,\pi^0$; 90-160 MeV) = 4.5 mb/sr and $\sigma(\pi^+,\pi^0$; 90-165 MeV) = 3.3 mb/sr for the energy-integrated 4° cross sections. One manifestation of the Coulomb force is the shift of the (π^+,π^0) spectrum to lower π^0 energies. Every state in ^{40}Sc is shifted up 12 MeV from its mirror state in ^{40}K. If one displaces the (π^+,π^0) spectrum to the right by 12 MeV to line up mirror

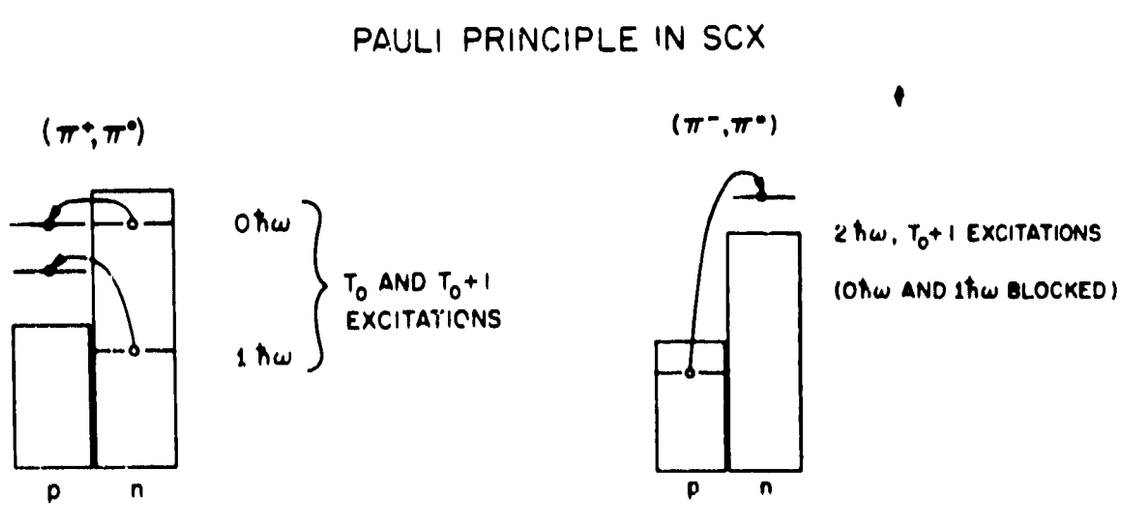

Fig. 12. The role of the Pauli exclusion principle in producing SCX asymmetries. The presence of 0- and 1-$\hbar\omega$ excitations in the (π^+,π^0) reaction increases the low-q cross sections compared to the (π^-,π^0) reaction.

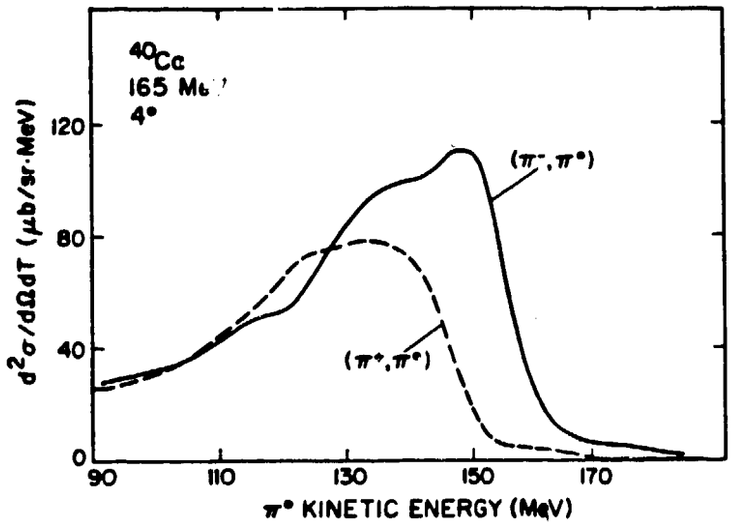

Fig. 13. Comparison of the (π^-,π^0) and (π^+,π^0) measured spectra (line traces) at 4° for ^{40}Ca. The (π^-,π^0) cross sections are larger in peak value and in the energy-integrated (90 to 165 MeV) value.

states, one would observe larger (π^-,π^0) cross sections in the peak region of the spectrum, compared to the (π^+,π^0) cross section.

Another feature of the ^{40}Ca data at low-q is the sizeable anisotropic component in the (π^-,π^0) cross sections that is not visible in the (π^+,π^0) cross sections (Fig. 8). This anisotropic component in the (π^-,π^0) reaction has made the extraction of the GDR cross section more dependent on the modeling of the background.

Coulomb effects can enter in several ways to produce π^-/π^+ SCX asymmetries in N = Z nuclei. The unbound neutron wave functions as produced in the (π^-,π^0) reaction will have a larger radial extent than the unbound proton wave functions as produced in the (π^+,π^0) reactions. This is due to the Coulomb barrier for protons. Since these pion reactions are highly surface peaked, we would expect an enhancement of the (π^-,π^0) cross sections. Also, Coulomb polarization of the ^{40}Ca ground-state proton and neutron densities can cause (π^-,π^0) enhancements. Auerbach has shown[28] recently that π^+/π^- SCX asymmetries for the GDR can be as large as 1.4 for $\sigma(\pi^-,\pi^0)/\sigma(\pi^+,\pi^0)$. Thus we see that the Coulomb force can also play a significant role in producing differences in the (π^+,π^0) and (π^-,π^0) cross sections at forward angles.

3. Shape Changes in the Low-q Spectra. The measured[22] angular variations in the $(\pi^\pm,\pi^0)$ spectra at forward angles are shown in Figs. 14 and 15 for ^{60}Ni, ^{140}Ce, and ^{208}Pb. It is clear from these spectra that an understanding of the background and its angular variation are required to extract individual multipole components. For ^{140}Ce and ^{208}Pb the spectra themselves

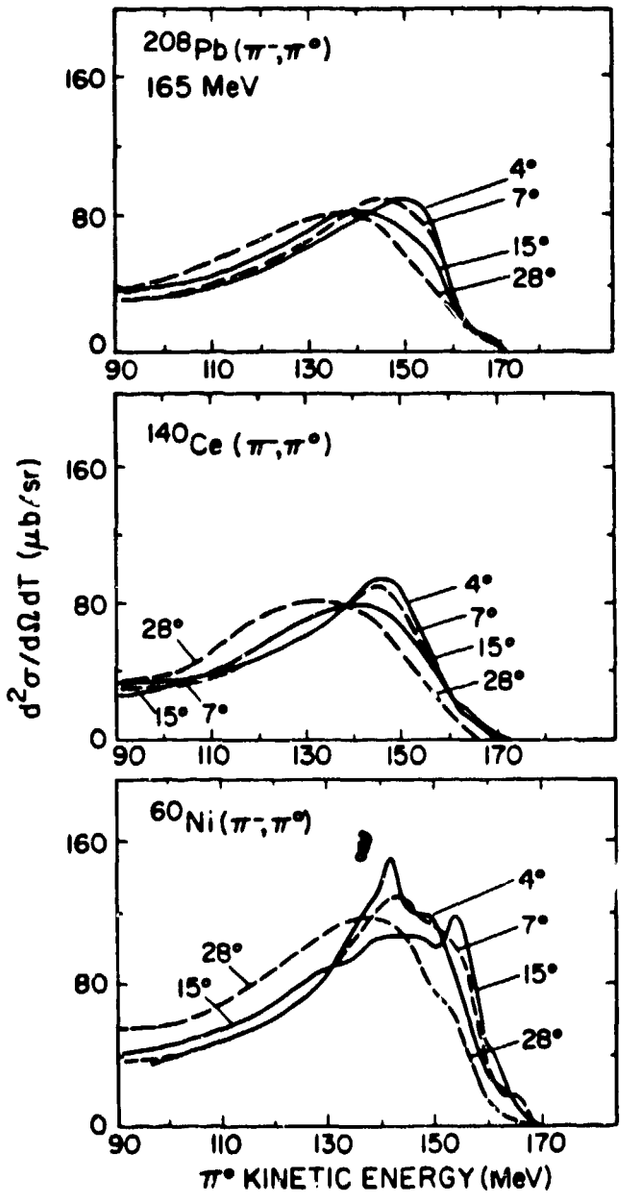

Fig. 14. Measured shape changes in the forward-angle spectra of the (π^-,π^0) reaction on ^{208}Pb, ^{140}Ce, and ^{60}Ni. The data are represented as line traces to allow for superposition of the spectra at different angles.

show no evident peaks. To give the relevant scale of angular variation we note that $\Delta L = 0$, 1, and 2 excitations at 165 MeV on ^{140}Ce are expected to have their peak cross sections at 0, 11, and 20°, respectively (DWIA calculations[29] with collective-model form factors). We see that the variations in the (π^-,π^0) spectra between 7 and 15° in the excitation-energy region of the monopole (near 146 MeV for ^{140}Ce) are comparable in magnitude to the monopole cross sections (Fig. 14). Between 7 and 15° the monopole cross sections are expected to be small ($\lesssim$0.1 mb/sr). Beyond 15° the measured cross

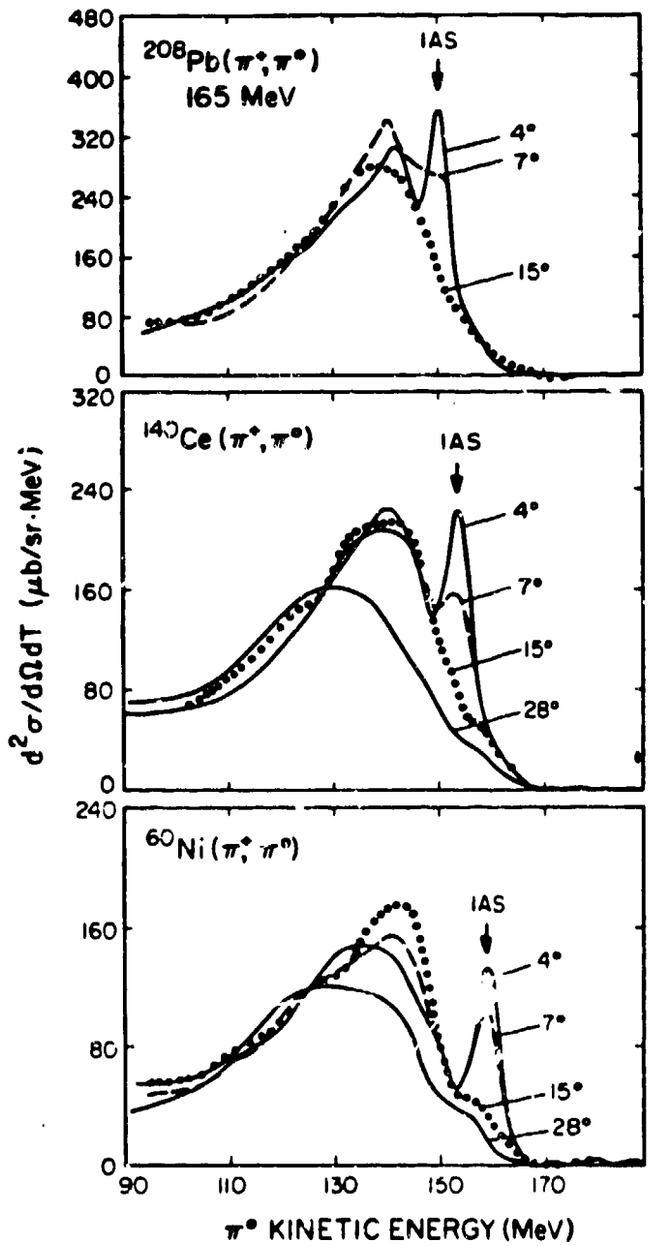

Fig. 15. Measured shape changes in the forward-angle spectra (line traces) of the (π^+,π^0) reaction on ^{208}Pb, ^{140}Ce, and ^{60}Ni.

sections in the monopole region continue to drop. Clearly one must have good accuracy in the treatment of the background to extract monopole cross sections. An analysis of these data based on a three-component ansatz (continuum + monopole + dipole) has been performed[22] and some of the results are discussed below.

As a general consideration, we note that in the angular range 0-30° and for energies 0 to 40 MeV, one might reasonably expect multipole components L = 0 to 4 to contribute. Angular-distribution shapes measured for states of

known J^{π} in inelastic pion scattering show[30] that natural-parity excitations do not follow pure Bessel-function shapes at forward angles. Relatively large forward-angle cross sections are observed for L = 0, 1, and 2 transitions. From nuclear-response-function calculations[31-33] we expect the major pieces of the L = 0 to 4 multipole distribution to occur between 0 and 40-MeV excitation.

C. Continuum + Monopole + Dipole Analysis

The analysis of the forward-angle π^0 spectra was performed[22] assuming that the spectra are composed of two giant resonances plus a continuum. The resonances were described as Gaussian functions with positions and widths to be determined from the fits. The background was represented as a product function of a Lorentzian shape times an exponential cutoff function. The exponential function constrains the continuum to go to zero near 165 MeV. The peak of the broad Lorentzian function (≈40 MeV FWHM) was set to the expected qf-scattering energy. The width of the function was allowed to vary with angle. Details of this analysis will be published in a forthcoming article.

The decompositions of the measured (π^-,π^0) 4° spectra given by this analysis are shown in Fig. 16. The individual monopole and dipole components and the summed C + M + D functions are shown with the data. The 4° spectra contain the maximum measured monopole signal.

The largest monopole cross section given by this analysis is for $^{40}Ca(\pi^-,\pi^0)^{40}K$. The 0° cross section is 0.8 ± 0.2 mb/sr. It has a large width Γ = 21.6 ± 1.9 MeV (FWHM) and it extends to excitation energies below the giant dipole resonance (Fig. 16). The centroid of monopole strength, projected into ^{40}Ca using the Coulomb displacement energy, is 29.9 ± 1.5 MeV. This is 9.9 MeV above the peak of the E1 photoabsorption spectrum (GDR).

The monopole excitation energies, projected into the target nucleus using Coulomb displacements are, for ^{60}Ni, ^{90}Zr, ^{120}Sn, ^{140}Ce, and ^{208}Pb, respectively, 33.0 ± 1.7, 32.3 ± 2.0, 33.5 ± 2.2, 33.5 ± 2.4, and 29.3 ± 2.8 MeV. The average value of all measured monopole energies is 31.9 MeV and the standard deviation is 1.9 MeV. Thus the T_0 + 1 monopole component is found to have a nearly constant excitation energy for nuclei from ^{40}Ca to ^{208}Pb.

Angular distributions that result from this analysis for ^{60}Ni and ^{140}Ce are shown in Fig. 17. The curves represent DWIA calculations employing the microscopic transition densities of Auerbach and Klein[32,33] and normalized to the data. The (π^-,π^0) cross section for the monopole is found to drop by a factor of approximately 3 between ^{60}Ni and ^{140}Ce. The dipole state could not be positively identified in (π^-,π^0) on ^{140}Ce and ^{208}Pb.

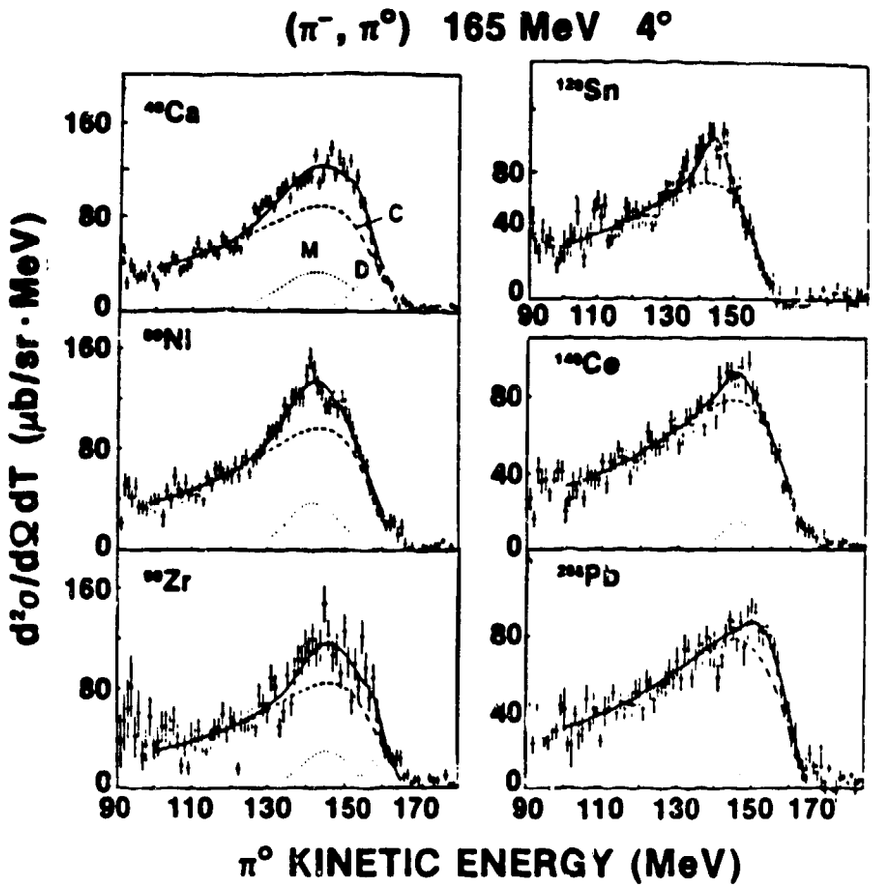

Fig. 16. The measured 4° spectra for the (π^-,π^0) reaction, shown with the decomposition into continuum (C) + monopole (M) + dipole (D) given by the analysis of Ref. 22.

The extracted 0° monopole cross sections for the (π^-,π^0) reaction on ^{40}Ca, ^{60}Ni, ^{90}Zr, ^{120}Sn, ^{140}Ce, and ^{208}Pb are, respectively, 0.77 ± 0.20, 0.73 ± 0.19, 0.63 ± 0.14, 0.53 ± 0.11, 0.23 ± 0.10, and 0.31 ± 0.09 mb/sr. They are seen to decrease with increasing A.

Monopole summary. The degree of confidence one may have in the extracted monopole parameters (E_x, Γ, $d\sigma/d\Omega$) depends on the degree of confidence one has in the characterization of the angular variations of the "nonresonant" background. Unfortunately, as may be seen by examining Figs. 14 and 16, the shapes of the (π^-,π^0) spectra at 165 MeV do not show sharp inflection points signaling the onset of the monopole resonances. The (π^-,π^0) data show an angular falloff from 4° to larger angles in the peak region of the spectra (Fig. 14). It is this feature that is identified with the monopole resonance on the basis of the inflection points observed[22,25] in a graph of $d\sigma/d\Omega$ vs q^2

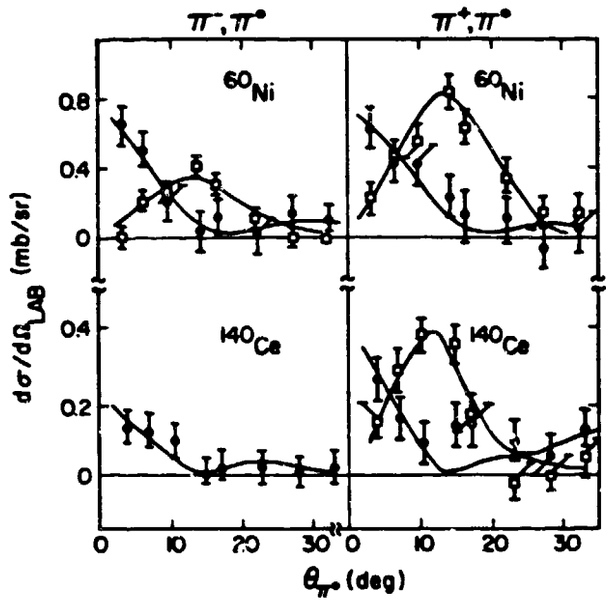

Fig. 17. The monopole and dipole angular distributions obtained in the analysis of Ref. 22. The solid lines are DWIA calculations with transition density calculated by Auerbach et al.[32,33]

for the cross sections integrated over energy intervals centered on the monopole states (identified in Fig. 16). Discussion of the assumptions and more details of the analysis will be available shortly.[22]

An unexpected result is the marginal quality of the monopole signal in ^{140}Ce and ^{208}Pb and its large value in ^{40}Ca and ^{60}Ni. This differs from the other giant resonances, which display their finest signatures in the heaviest nuclei.

We are making measurements in Los Alamos at 120 and 230 MeV to determine if the signal/background for the monopole resonance can be improved.

Dipole summary. In the (π^-,π^0) reactions the GDR is observed directly as a peak in the measured spectra for nuclei ^{40}Ca to ^{120}Sn. The peak values of the differential cross sections drop from ≈1 mb/sr for ^{40}Ca to 0.15 ± 0.03 mb/sr for ^{120}Sn. The Pauli blocking for the $T_0 + 1$ component is thereby clearly demonstrated. For the (π^+,π^0) reaction a GDR peak is directly visible for nuclei ^{40}Ca to ^{120}Sn. The extracted peak cross sections are approximately 1 mb/sr, independent of A. The role of the Pauli principle again is evident. The isospin-splitting energies $E(T_0 + 1) - E_0(T_0 - 1)$ are at present not measured with sufficient accuracy to yield new information. They are consistent with previous measurements. The demonstrated existence of the dipole signal in both (π^-,π^0) and (π^+,π^0) reactions makes future studies of SCX asymmetries vs N − Z for the GDR look quite promising.

Isovector quadrupole. The $(\pi^{\pm},\pi^{0})$ data do not show directly discernable $L = 2$ components, which are expected to have maximum cross sections near 25° for ^{140}Ce and near 20° for ^{208}Pb. Apparently this multipole distribution is too broad and/or too weak relative to the combined strength of all the other multipoles to produce a clear signature in the $(\pi^{\pm},\pi^{0})$ spectra. To test for its presence, a constrained fit with a (continuum + monopole + dipole + quadrupole) ansatz was performed.[22] The quadrupole was constrained to an $L = 2$ angular-distribution shape and an excitation energy and width given by theory.[31-33] This constrained fit produced no evidence for a quadrupole component. Thus at present the $(\pi^{\pm},\pi^{0})$ data cannot be used to determine the properties of the isovector quadrupole resonance.

IV. INELASTIC PION SCATTERING

Inelastic pion scattering at beam energies near 165 MeV favors isoscalar transitions four to one over isovector transitions due to the nature of the πN force. Therefore, inelastic scattering is most suitable for study of the isoscalar resonances. The most promising work to date are π^{+}/π^{-} comparisons for the isoscalar quadrupole resonance (GQR). Results have been reported[34-36] for ^{40}Ca, ^{89}Y, ^{118}Sn, and ^{208}Pb.

An interesting result is the large value of $R \equiv \sigma(\pi^{-})/\sigma(\pi^{+})$ measured for the GQR. The measured values[35] are $R = 1.9$ for ^{118}Sn at 130 MeV and[36] $R = 3.0$ for ^{208}Pb at 162 MeV. One may expect values given by

$$R \equiv \frac{\sigma(\pi^{-})}{\sigma(\pi^{+})} \approx \left(\frac{3N + Z}{N + 3Z}\right)^{2} \tag{8}$$

for pion energies near the Δ resonance. This equation assumes equal-amplitude neutron and proton oscillations $[(\beta R)_n = (\beta R)_p = (\beta R)]$, which gives $M_n = N(\beta R)$ and $M_p = Z(\beta R)$ for the collective-model neutron (M_n) and proton (M_p) transition matrix elements. Equation (8) gives R values 1.37 for ^{118}Sn and 1.54 for ^{208}Pb. Thus the large measured values are a puzzle.

Explanations for the large R values have been discussed[35,36] in terms of neutron haloes in the ground-state densities and medium modifications of the πN force. Estimates indicate that reasonable modifications along these lines do not affect R sufficiently to bring theory into agreement with the data.

Spectra for $^{208}Pb(\pi,\pi')$ reactions are shown in Fig. 18. The expected maximum for an $L = 2$ angular distribution is near 20°. The GQR has a previously measured excitation energy of 10.5 MeV. A peak is seen at this energy in both the π^{+} and π^{-} spectra. A striking feature of these spectra is that

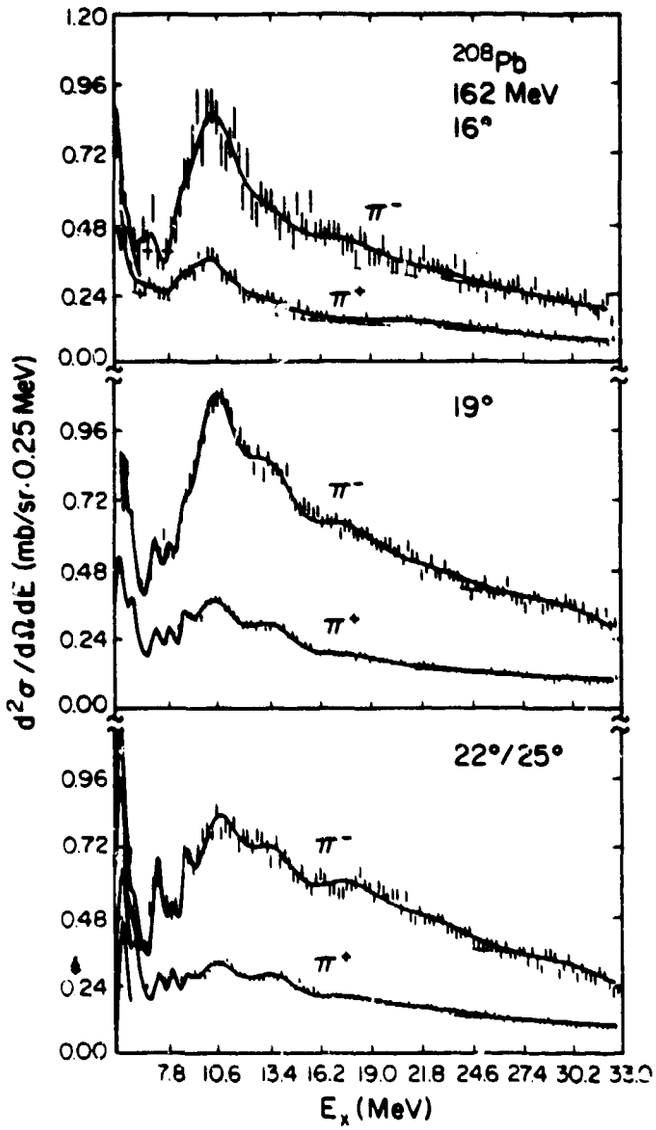

Fig. 18. Measured[36] inelastic π^- and π^+ spectra for ^{208}Pb. The π^- double-differential cross section $d^2\sigma/d\Omega dT$ is approximately 3 times that of the π^+ scattering for excitation energies between 7 and 33 MeV. Possible explanations for this large π^-/π^+ asymmetry are discussed in the text.

$\sigma(\pi^-) \approx 3\sigma(\pi^+)$, nearly independent of excitation energy for $E_x > 7$ MeV. Thus the ratio $R = 3.0$ reported[36] for the GQR holds approximately for all unbound states. For the bound states the values R are smaller[35,36]: $R = 1.3 \pm 0.1$ for the 2_1^+ in ^{118}Sn and $R = 1.8 \pm 0.1$ for the 3_1^- state in ^{208}Pb. These results are highly suggestive of a continuum effect that enhances $\sigma(\pi^-)$ over $\sigma(\pi^+)$ and affects all unbound states up to 30-MeV excitation.

A possible explanation would seem to be in the differences in unbound neutron and proton wave functions. The Coulomb barrier for protons in ^{208}Pb is ≈16 MeV and the proton separation energy for ^{208}Pb is $S_p = 8.0$ MeV. The

neutron separation energy is $S_n = 7.4$ MeV. Thus for excitation energies between 7.4 and ≈24 MeV, the neutron wave functions have a larger radial extent than the proton wave functions. For the strongly absorbed pions this will lead to larger π^- cross sections. Calculations with continuum wave functions are required to determine the size of the effect. Qualitatively, we would expect $\sigma(\pi^-)/\sigma(\pi^+)$ to approach N/Z at very high excitation energies where neutron and proton wave functions are similar. Also, the pion asymmetries should be less for lighter nuclei where the Coulomb barrier is lower. The presently available data are not inconsistent with these expectations.

If indeed the measured R values are dominated by continuum effects, it will be difficult to extract reliable isovector-to-isoscalar transition amplitudes for unbound giant-resonance states.

V. SUMMARY

We have followed in this article the highlights of the recent extensive research with pions on nuclear giant resonances. I believe we have the following results.

(1) The IAS and DIAS transitions can be measured throughout the periodic table. The basic patterns of forward-angle cross sections are determined and are partially understood. This paves the way for possible new insights to nuclear structure using these transitions.

(2) There is a forward-peaked feature in the (π^-,π^0) cross sections, which may be due to an isovector monopole resonance. Further understanding of the background is required to accurately identify this component.

(3) The $(\pi^\pm,\pi^0)$ reactions provide an excellent tool for study of the charge-exchange generalizations of the E1 photoabsorption resonance (GDR) since there are peaks in the spectra whose area extraction is not highly model dependent.

A large number of experimental results presented are from the LAMPF π^0 spectrometer group. I wish to thank the members for many informative discussions and for the help given in preparation of this article. I have benefited especially from many discussions with my colleague, J. D. Bowman, although our interpretations on the isovector monopole results do not coincide completely.

A special thanks goes to Margaret Pinyan for her competent assistance in the preparation of this manuscript.

REFERENCES

1. M. B. Johnson and H. Bethe, Comments Nucl. Part. Phys. 8, 75 (1978).
2. M. B. Johnson, Phys. Rev. C 22, 192 (1980).
3. H. W. Baer et al., Phys. Rev. Lett. 45, 982 (1980).
4. F. Irom et al., Phys. Rev. C 28, 2565 (1983); and Irom et al., to be published (^{7}Li).
5. U. Sennhauser et al., Phys. Rev. Lett. 51, 1324 (1983).
6. A. Doron et al., Phys. Rev. C 26, 189 (1982); and Phys. Rev. Lett. 48, 989 (1982).
7. M. D. Cooper et al., Phys. Rev. Lett. 52, 1100 (1984).
8. S. J. Greene et al., to be published.
9. M. B. Johnson and E. R. Siciliano, Phys. Rev. C 27, 730 (1983) and Phys. Rev. C 27, 1647 (1983).
10. W. R. Kaufman and W. R. Gibbs, Los Alamos National Laboratory report LA-UR-83-736, to be published.
11. P. A. Seidl et al., Phys. Rev. Lett. 50, 1106 (1983); P. A. Seidl, Los Alamos National Laboratory documents LA-UR-84-17 (1983) and LA-UR-9709-PR.
12. C. L. Morris et al., Phys. Rev. Lett. 45, 1233 (1980).
13. K. K. Seth, Proc. Int. Symp. on Electromagnetic Properties of Atomic Nuclei, Tokyo, Japan, November 1983 (to be published).
14. S. J. Greene et al., Phys. Rev. C 25, 927 (1982).
15. G. Miller and J. E. Spencer, Ann. Phys. 100, 562 (1976).
16. M. Kaletka, Ph.D. thesis, Northwestern University, 1983, Los Alamos National Laboratory document LA-9947-T (1984).
17. R. Gilman, private communication.
18. A. Gal, Phys. Rev. C 25, 2680 (1982).
19. R. D. Evans, in The Atomic Nucleus (McGraw-Hill, New York, 1955), p. 293.
20. H. W. Baer et al., Phys. Rev. Lett. 49, 1376 (1982).
21. J. D. Bowman et al., Phys. Rev. Lett. 50, 1195 (1983).
22. A. Erell et al., Phys. Rev. Lett. (in press); and to be published.
23. H. W. Baer et al., Nucl. Phys. A 239, 437c (1983).
24. J. A. Alster, Proc. 16th LAMPF Users Group Meeting, July 1982, Los Alamos National Laboratory report LA-9767-C.
25. J. D. Bowman, Proc. Int. Symp. on Highly Excited States and Nuclear Structure, Orsay, France, September 4-8, 1983 (HESANS-83) (to be published).
26. D. Ashery et al., Phys. Rev. Lett. 50, 482 (1983); and to be published.
27. C. H. Q. Ingram et al., Phys. Rev. C 27, 1578 (1983); and C. H. Q. Ingram, Proc. Symp. on Delta-Nucleus Dynamics, Argonne National Laboratory, Argonne, Illinois, May 2-4, 1983, Argonne National Laboratory report ANL-PHY-83, CONF-830588.
28. N. Auerbach, Phys. Rev. Lett. 49, 913 (1982).
29. E. R. Siciliano, private communication (1983).
30. C. L. Morris, Proc. Symp. on Delta-Nucleus Dynamics, Argonne National Laboratory, Argonne, Illinois, May 2-4, 1983, op. cit., p. 101; and M. Theis, ibid., p. 115.
31. D. Gogny, HESANS-83 (to be published).
32. N. Auerbach, HESANS-83 (to be published).
33. N. Auerbach et al., Phys. Rev. C 29, 526 (1984).
34. J. Arvieux et al., Phys. Rev. Lett. 42, 753 (1979); and J. Arvieux et al., Phys. Lett. 90B, 371 (1980).
35. J. L. Ullmann et al., Phys. Rev. Lett. 51, 1038 (1983).
36. C. L. Morris et al., HESANS-83 (to be published); and S. Seestrom-Morris, private communication.